

Oil Palm Nutrient Mapping Using Multispectral Drone

Nurul Syafiza Mohd Jefri¹, Nurarina Mohd Amir¹, Abd Wahid Rasib^{1*}, Anuar Ahmad¹,
Norhadija Darwin¹ and Wan Mohd Hairy Wan Yusof²

¹Geoinformation Programme, Faculty of Built Environment and Surveying,
Universiti Teknologi Malaysia, 81310 Johor Bahru, Johor, Malaysia

²Tradewinds Plantation Berhad, Bukit Kledek Estate, Gemencheh, Negeri Sembilan, Malaysia

*Corresponding author: abdwahid@utm.my

Abstract – Unmanned Aerial Vehicle (UAV) is one of the platforms that have recently proven profitable in agriculture, despite being more commonly used as a carriage platform. Nevertheless, the use of UAVs for mapping promotes precision agriculture. Foliage mapping and nutrient mapping are examples of mapping techniques that are beneficial for oil palm. Assessing the condition and distribution of nutrient content is essential for plantation management to monitor the health of the trees, identify potential problems such as nutrient deficiency or pest infestation, and optimise management practices for higher yields. Therefore, this study aims to produce nutrient content information from UAV and spectroradiometer data. Compact remote sensing sensors operating at visible (RGB) (0.4-0.7 micrometre), Near Infra-red (NIR) (0.7-1.2 micrometre), thermal infrared (TIR) and Long-wave Infrared (LWIR) bands (7-14 micrometre) were used in this study to determine the concentration of foliage content in the oil palm plantation. Nutrient elements such as Nitrogen (N), Phosphorus (P), Potassium (K), Calcium (Ca), and Magnesium (Mg) were detected from the foliar content as indicated in the 17th frond of oil palm leaves. This study successfully developed a method for identifying and quantifying the nutrient content of oil palm plantations using a drone platform. This study would aid in predicting oil palm production and provide farm owners and managers with valuable decision-making information.

Keywords – Unmanned Aerial Vehicle (UAV), Oil Palm, Nutrient, Foliage

©2023 Penerbit UTM Press. All rights reserved.

Article History: Received 11 June 2023, Accepted 26 July 2023, Published 30 August 2023

How to cite: Mohd Jefri, N.S., Mohd Amir, N., Rasib, A.W., Ahmad, A., Darwin, N., and Wan Yusof, W.M. H. (2023). Oil Palm Nutrient Mapping using Multispectral Drone. Journal of Advanced Geospatial Science and Technology. 3(2), 145-175.

1.0 Introduction

Oil palm (*Elaeis guineensis Jacq.*) is one of Malaysia's primary commodity crops, mostly planted for the industrial manufacture of vegetable oil due to their advantages in having suitable land temperature and rainfall frequency [1]. Furthermore, since oil palm is Malaysia's primary source of biomass or dry matter, it needs a lot of macro and micronutrients for growth and yields. Thus, oil palm requires sufficient nutrients in the proper proportion to produce good and remain healthy over time. Although soil contains specific nutrients, it is frequently imbalanced and lacks sufficient nutrients to support the growth and production of oil palm [2].

Conventionally, nutritional content information is gathered through soil and oil palm leaf analysis, which entails damaging chemical analysis methods and having an agronomist observe leaves, stems, and trees to diagnose nutrient deficits and illnesses. Leaf analysis more accurately represents oil palm tree consumption from frond 3 (F3), frond 9 (F9), and frond 17 (F17). Palm oil production relies heavily on the oil palm's nutrient content, as it is through photosynthesis that the tree synthesizes carbohydrates and other essential compounds that contribute to the growth and development of the palm fruit bunches [3]. The health and density of the foliage are crucial indicators of the overall vitality and productivity of the oil palm plantation [8]. To help farmers meet their agronomic, economic, and environmental goals, it is important to have a thorough understanding of their crop's nutrient needs across its life cycle. This will allow for the development of effective nutrient management plans [8].

In recent years, conventional methods or manual monitoring in oil palm growth surveillance is no longer practicable because of the development of remote sensing technology such as ground-based airborne and satellite that can be used as it saves cost, time and energy, and is capable of improving the likelihood of plant classification using spectral and textural analysis [7]. Effective plantation management and the environmental impacts of oil palm farms can be better understood with the help of remote sensing. In addition, green biomass, nutritional status, pigment degradation, and photosynthetic efficiency can all be evaluated using multispectral cameras, which gather just a small number of spectral bands simultaneously in the visible to near-infrared (VIS-NIR) range. [1,5]. Meanwhile, to assess an object's characteristics without damaging it, a spectrometer or spectroradiometer measures the spectrum of light reflected off it. This spectrometer's exceptional features have made it a valuable resource for researchers in many disciplines, including agriculture. [9,10].

In the field, UAVs are frequently employed for collecting low-altitude aerial data at large coverage. It is identified as a potential technology that can generate high spatial resolution imagery (less than 1m) at a temporal frequency that offers rapid reactions to provide crop and field status information. One of the main reasons why the UAV industry has surpassed market demand is that small UAVs are part of Low Altitude Remote Sensing (LARS), which is cheaper than traditional manned aircraft. [12]. Oil palm growers can benefit from data-driven techniques for early and accurate yield estimation and health assessment due to the ability of unmanned aerial vehicles (UAVs) to collect higher-resolution aerial images at a significantly lower cost compared to piloted aeroplanes and satellite imaging [3,6].

An orthophoto can be produced by combining the NIR and RGB images. Thus, utilizing the orthophoto images and spectroradiometer data, the analysis of the vegetation can be conducted by analyzing the spectral response curve and vegetation indices such as Normalized Difference vegetation index (NDVI) as well as Modified Soil-adjusted Vegetation Index (MSAVI) [12]. Thus, a thermal infrared (TIR) image can obtain the quantitative surface temperature information through the different land use/land cover categories to determine the trend of nutrient contents [8]. Thus, this study aims to use drone-based remote sensing data and spectroradiometer measurement equipped to obtain information on the nutrient content of the oil palm for proper tree growth and development.

2.0 Methodology

2.1 Study Areas

The study area is Bukit Kledek Estate, located approximately 2°27'45" N in latitude and 102°30'0.7" E in longitude of Gemencheh, Negeri Sembilan. The estimated terrain elevation above sea level is 66 metres. Bukit Kledek Estate was planted with oil palm trees covering approximately 865.80 ha. This study will involve about 12 acres of the experimental plot for data collection, and 25 selected oil palm trees in the plantation will be observed using a spectroradiometer in data sampling. The Estate had arranged the data collection area as they are a private company, and an outsider needs to follow the requirements. This experimental plot indicates the undulating terrain was able to determine the oil palm nutrient uptake at lower and upper ground levels. The location of the study area and terrain pattern are shown in Figure 1 and Figure 2 below.

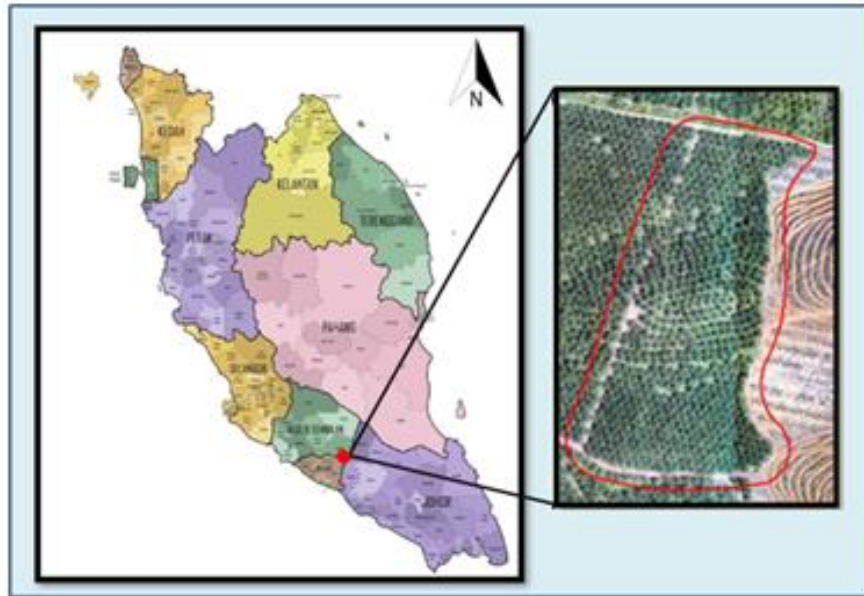


Figure 1. Location of the study area

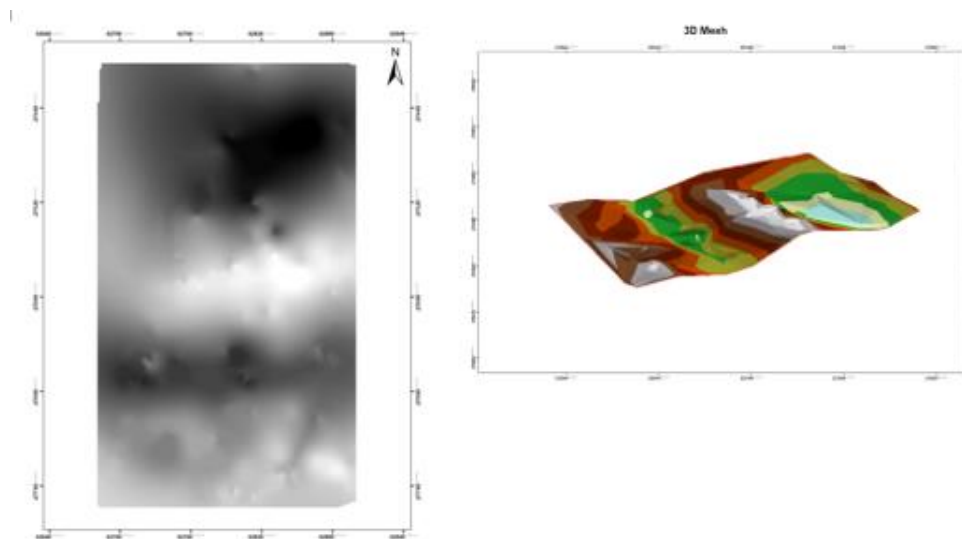


Figure 2. Digital Terrain Model and 3D Mesh of study area

2.2 Data Acquisition

This study's data acquisition process comprises RGB, NIR, and TRI sensors. The images were acquired through fieldwork conducted with a DJI Phantom 4 drone equipped with a MAPIR Survey 2 NIR and RGB sensor for RGB and NIR data acquisition. Phantom 4 will be attached for thermal images with DJI Zenmuse XT (Table 2). In collecting the spectroradiometer data, the oil palm

tree's branches (Figure 3) need to be cut for spectral observation (Figure 4) and to produce the spectral response graph. The 17th fronds of the palm tree were chosen for spectroradiometer observation in this study to indicate oil palm growth trends [15].



Figure 3. 25 samples of oil palm leaves

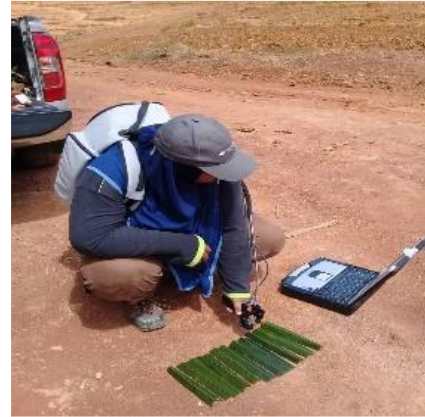






Figure 4. Spectroradiometer observation

Therefore, 25 different oil palm tree branches randomly representing the lower stream and upper stream were used in this study area. Subsequently, GPS observation is also carried out in selected areas to obtain the Ground Control Point (GCP) with coordinate references using Topcon GR-5. The Real-Time Kinematic (RTK) method acquired field data to establish ground control points (GCP). A total of 12 GCPs and 25 points for a sample has been collected. Table 1 shows the coordinates of the GCPs point.

Table 1. Coordinate of the GCPs

Point	Latitude	Longitude
GCP 01	2° 27' 38.819"	102° 30' 18.256"
GCP 02	2° 27' 39.319"	102° 30' 15.606"
GCP 03	2° 27' 39.460"	102° 30' 13.424"
GCP 04	2° 27' 40.468"	102° 30' 18.950"
GCP 05	2° 27' 45.781"	102° 30' 18.709"
GCP 06	2° 27' 44.773"	102° 30' 13.946"
GCP 07	2° 27' 42.631"	102° 30' 12.956"
GCP 08	2° 27' 40.489"	102° 30' 12.344"
GCP 09	2° 27' 41.090"	102° 30' 15.844"
GCP 10	2° 27' 42.955"	102° 30' 18.205"
GCP 11	2° 27' 44.921"	102° 30' 17.399"
GCP 12	2° 27' 44.582"	102° 30' 18.652"

Table 2. The instruments used in this study

Instrument	Specifications
<p>(a)</p>  <p>DJI Phantom 4 Drone</p>	<p>Payload: 1.38 kg Flight Autonomous: 28 minutes Velocity Range: 2 m above ground Altitude Range: 0 - 10 m Operating Range: 0 - 10 m Obstacle Sensory Range: 0.7 - 15 m</p>
<p>(b)</p>  <p>Survey3W MAPIR Camera - Visible Light RGB & Near Infrared (NIR)</p>	<p>Focal length: 35 mm Sensor: 20 megapixels FOV: 60 (horizontal) Capture Speed: RAW+JPG: 3 Seconds / Photo. JPG: 2 Seconds / Photo</p>
<p>(c)</p>  <p>DJI XT Zenmuse Thermal Camera</p>	<p>Lens: 13 mm Resolution: 640 × 512 pixels Spatial Resolution: 0.4 cm Spectral Range: 7.5 – 13.5 micrometre Thermal Imager: Uncooled VOx Microbolometer</p>
<p>(d)</p>  <p>Spectral Evolution RS-3500 Series Field Portable Spectroradiometer</p>	<p>Spectral Range: 350 – 2500nm Spectral Resolution 3nm @700nm, 8nm @1500nm, 6nm @2100nm Wavelength Accuracy: ~0.5 bandwidth Batteries: External Li-ion battery and universal power charger Weight: 7.3 lbs (spectroradiometer only)</p>

e)



Topcon Tripod

GPS

Signals Tracked GPS, GLONASS, QZSS, SBAS,
Galileo* and Beidou (BDS)*

Number of Channels 226-Channel Vanguard
Technology™ with Universal Tracking Channels

Accuracy:

RTK H: 10mm + 1.0ppm

V: 15mm + 1.0ppm

Static H: 3mm + 0.5ppm

V: 5mm + 0.5ppm

2.3 Data Pre-Processing

In the data pre-processing stage, several processes need to be performed: image stitching, layer stacking, orthophoto, geometric correction, and radiometric correction, which involves converting to reflectance, topography DSM/DTM, and thermal image. At the same time, conversion to reflectance is carried out based on linear correlation orthophoto and spectroradiometer data. The raw data from RGB, NIR, and IRT sensors will go through stitching, in which the images from each sensor are combined into a single, unified image format known as an orthophoto. Figure 5 shows the orthophoto of RGB, NIR and IRT successfully produced through image processing systems such as Pix4D Mapper Software and Agisoft.

All orthophotos must be geometrically corrected to correct geometric distortions from a distorted image and transform the data to real-world coordinates on the Earth's surface. Next, to ensure that the data accurately represents the reflected or emitted radiation detected by the sensor, radiometric correction must be conducted to adjust the data for abnormalities in the sensor and undesirable sensor or ambient noise. Other than that, the Digital Terrain Model (DTM) or Digital Surface Model (DSM) is produced during processing step 3, DSM, Orthomosaic and Index. Once the Raster DSM is generated, the tiles of the Raster DSM are merged.

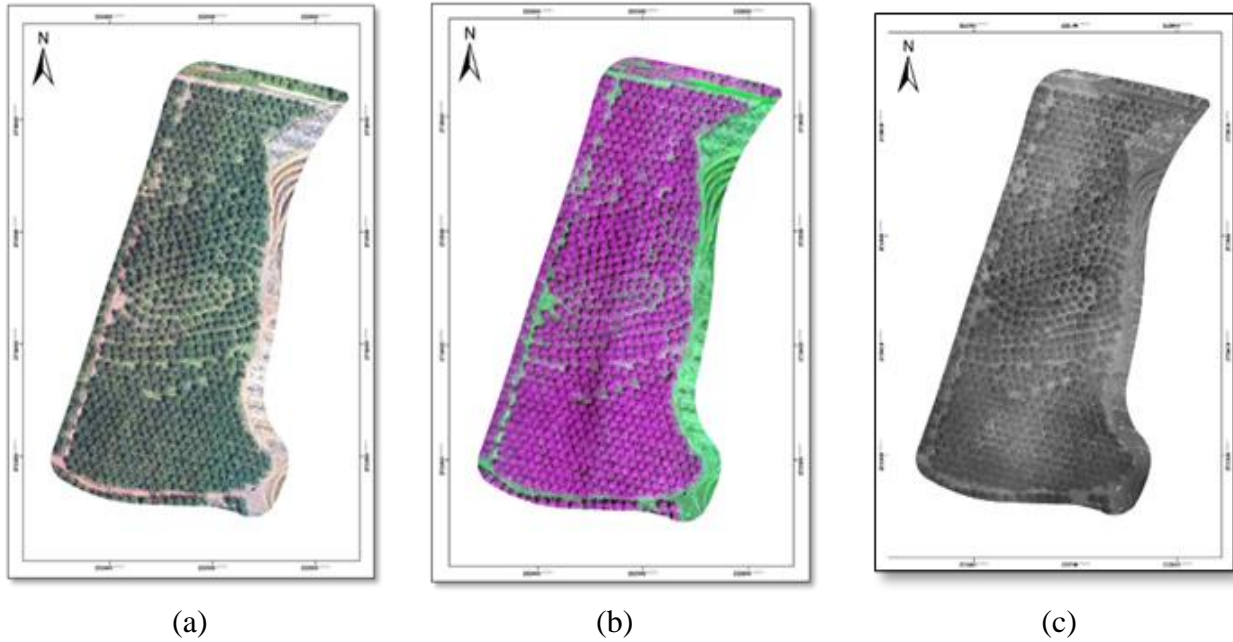


Figure 5. The result of the ortho mosaic of (a) RGB, (b) NIR and (c) thermal image

2.4 Data Processing

Data processing is a stage that has been done to obtain the final output of this research and the analysis. In this stage, the spectral reflectance of oil palm trees was used to generate the reflectance graph for UAV and spectroradiometer. The primary data, the orthophoto image, will be processed using GIS and remote sensing software such as ArcGIS and QGIS. Furthermore, this study used the NIR and red spectrums to estimate Normalized Different Vegetation Index (NDVI) Modified Soil Adjusted Vegetation Index (MSAVI) maps. These maps were produced to analyze the oil palm trees in the study area. Then, the NDVI and MSAVI process is performed by using the Raster Calculator tool in ArcGIS ArcMap 10.3 software. Below are the equations [8] to determine NDVI and MSAVI values.

$$\begin{aligned}
 \text{NDVI} &= (\text{NIR} - \text{RED}) / (\text{NIR} + \text{RED}) \\
 \text{MSAVI} &= (1+L) * (\text{NIR} - \text{RED}) / (\text{NIR} + \text{RED} + L) \qquad \qquad \qquad \text{(equation 1)}
 \end{aligned}$$

However, the difference between SAVI and MSAVI comes in how L is calculated. MSAVI uses the following formula to calculate L:

$$L = 2 * s * (\text{NIR} - \text{Red}) * (\text{NIR} - s * \text{Red}) / (\text{NIR} + \text{Red}) \qquad \qquad \qquad \text{(equation 2)}$$

where s is the slope of the soil line from a plot of red versus near-infrared brightness values.

For foliage modelling, the main elements of nutrients involved are Nitrogen (N), Phosphorus (P), Potassium (K), Calcium (Ca) and Magnesium (Mg). The regression models indicate that nutrients and reflectance have a positive relationship, and the amount of nutrients can be estimated using the reflectance values at various bands. By using the reflectance data and foliar analysis data, regression analyses using the models by [8] (see equation 3) were performed to show the relationship between the nutrient element and the bands.

$$\begin{aligned}
 N &= 2.405b_0 - 18.042b_1 + 12.995b_2 + 6.299b_3 - 0.0507b_4 \\
 P &= 0.161b_0 - 1.219b_1 + 0.07971b_2 + 1.06b_3 + 0.003676b_4 \\
 K &= 1.277b_0 + 25.557b_1 + 6.351b_2 - 30.531b_3 - 0.581b_4 \\
 Ca &= 0.654b_0 - 13.924b_1 + 5.75b_2 + 4.635b_3 + 0.09429b_4 \\
 Mg &= 0.138b_0 + 1.579b_1 - 0.354b_2 + 2.524b_3 - 0.171b_4
 \end{aligned}
 \tag{equation 3}$$

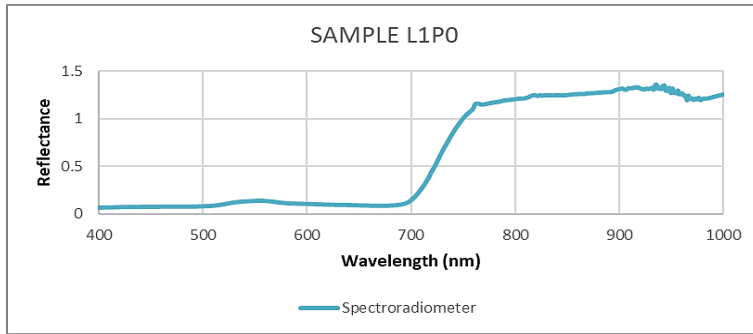
Where;

b = Band	X = Reflectance
b_1 = Band 1	N = % concentration of nitrogen
b_2 = Band 2	P = % concentration of phosphorus
b_3 = Band 3	K = % concentration of potassium
b_4 = Band 4	Ca = % concentration of calcium
Mg = % concentration of magnesium	

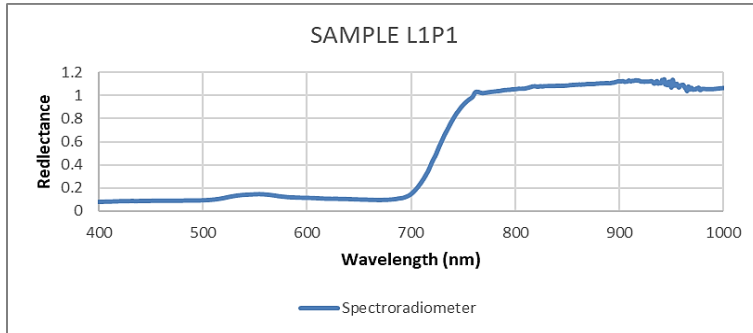
3.0 Results and Discussions

3.1 Spectral Reflectance Curve Graph

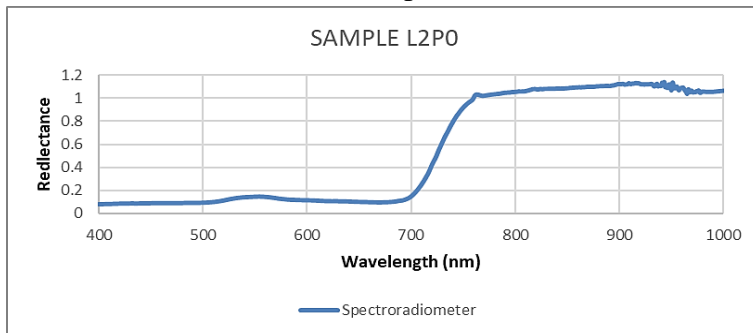
The spectral reflectance curves for all 25 samples of frond 17 obtained from the spectroradiometer are shown in Figure 6 (a-y). In general, most samples show similar spectral reflectance curves where nearly all of the samples chosen are in healthy condition. Thus, the graph showed the highest reflectance in the near-infrared band, approximately from 0.753 – 0.900 μm wavelengths.



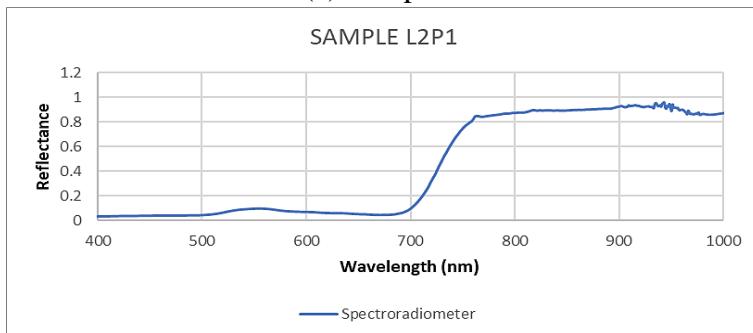
(a) Sample 1



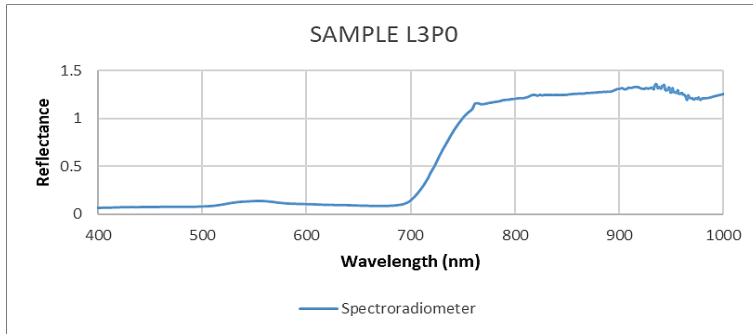
(b) Sample 2



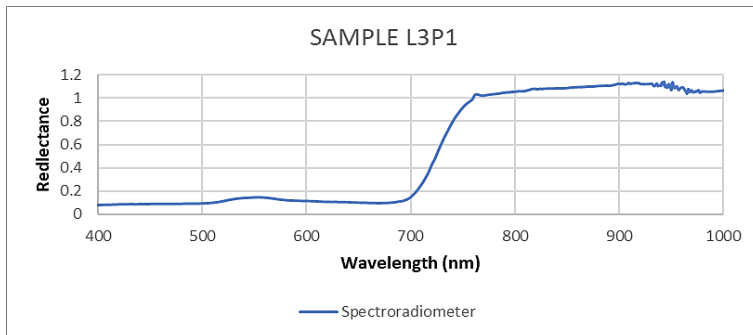
(c) Sample 3



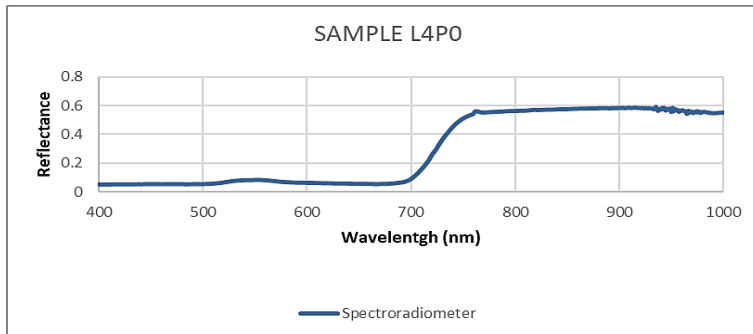
(d) Sample 4



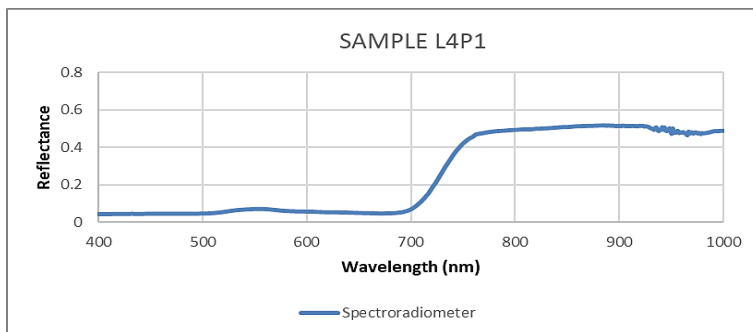
(e) Sample 5



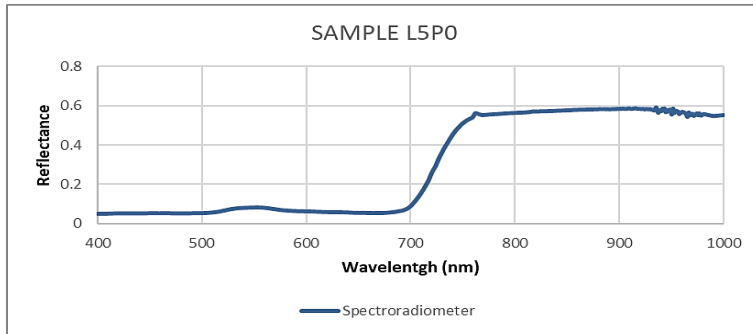
(f) Sample 6



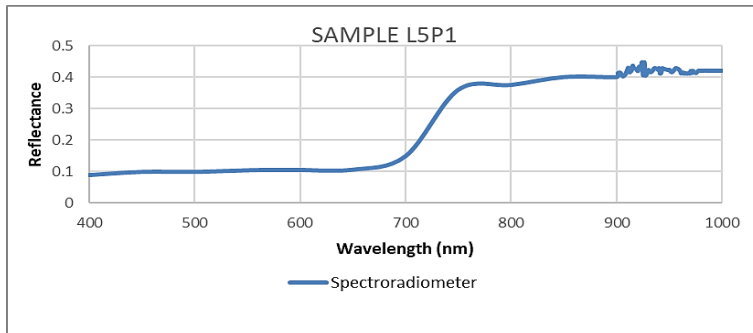
(g) Sample 7



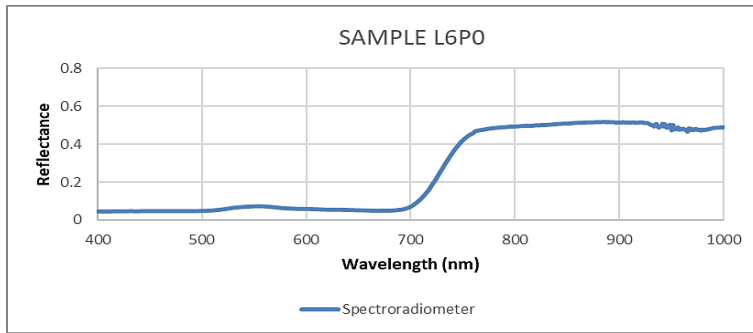
(h) Sample 8



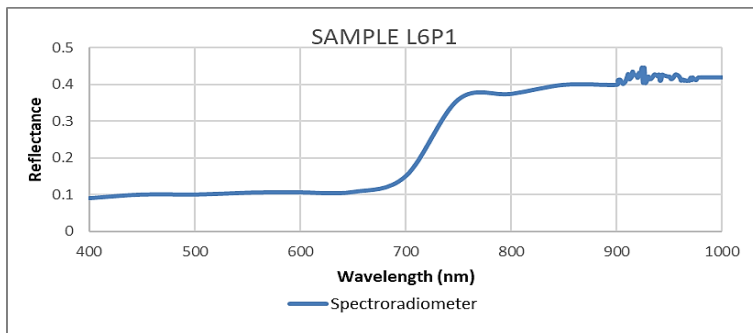
(i) Sample 9



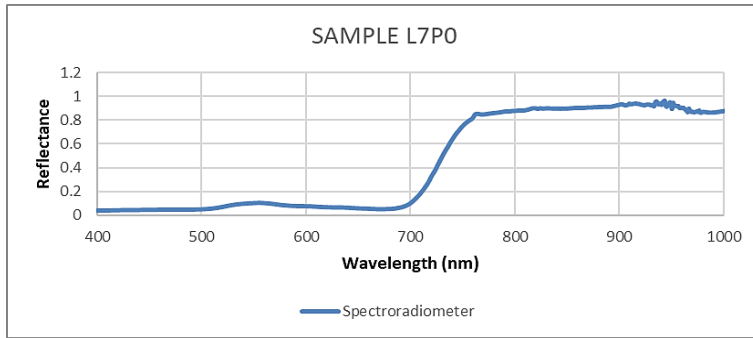
(j) Sample 10



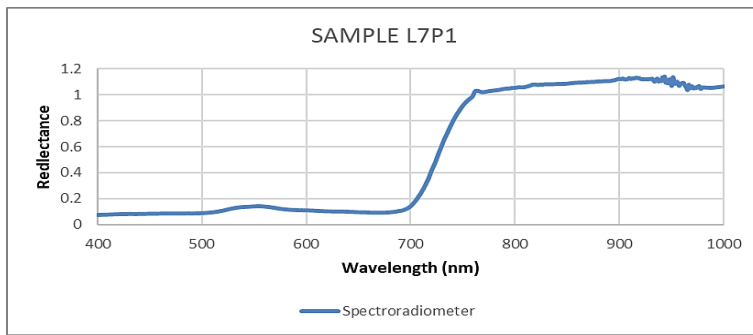
(k) Sample 11



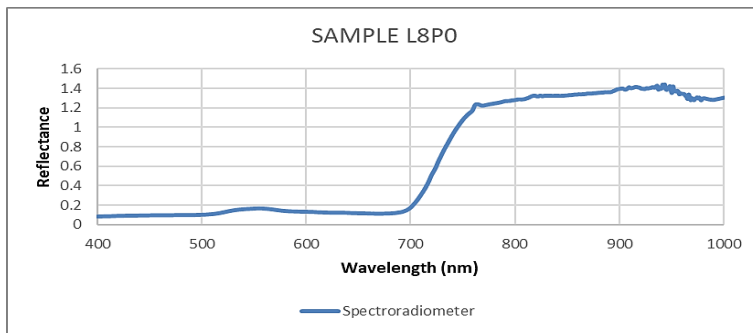
(l) Sample 12



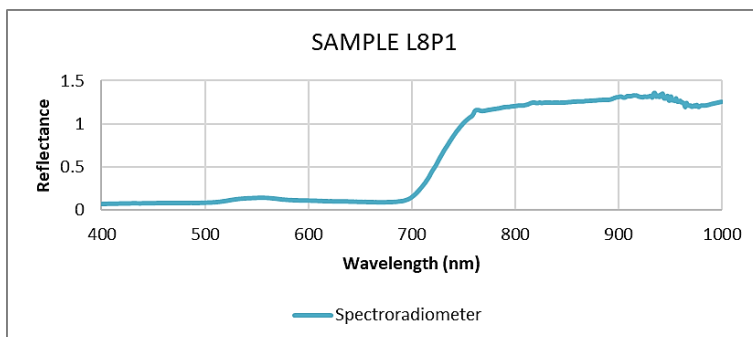
(m) Sample 13



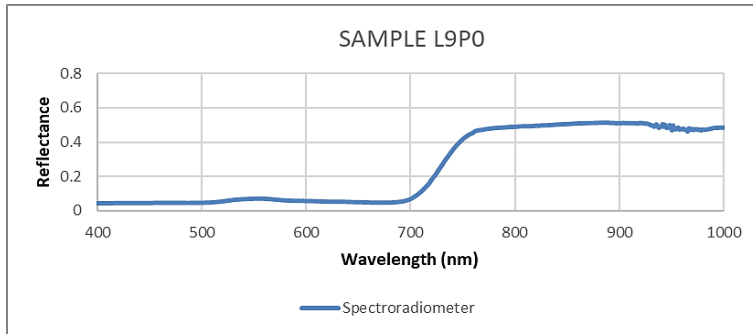
(n) Sample 14



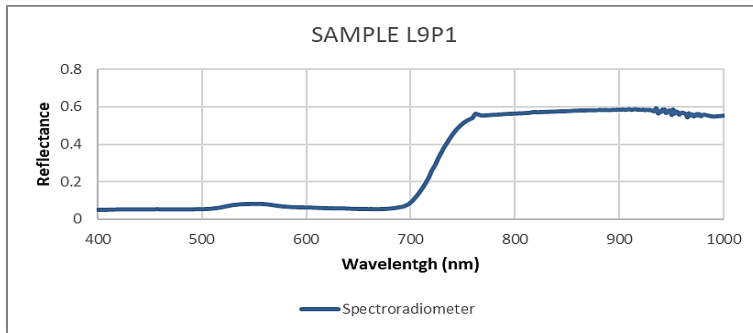
(o) Sample 15



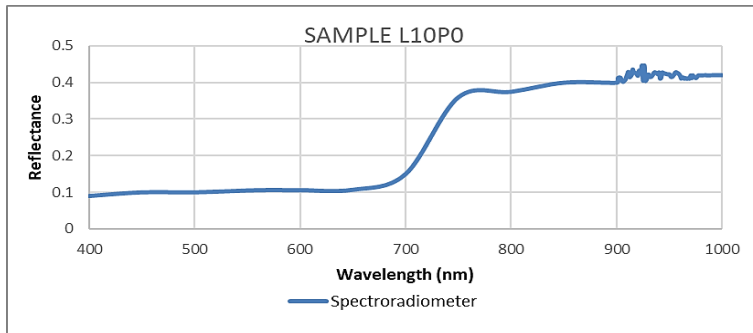
(p) Sample 16



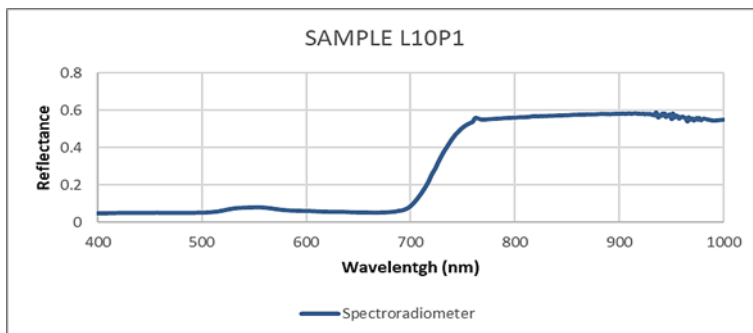
(q) Sample 17



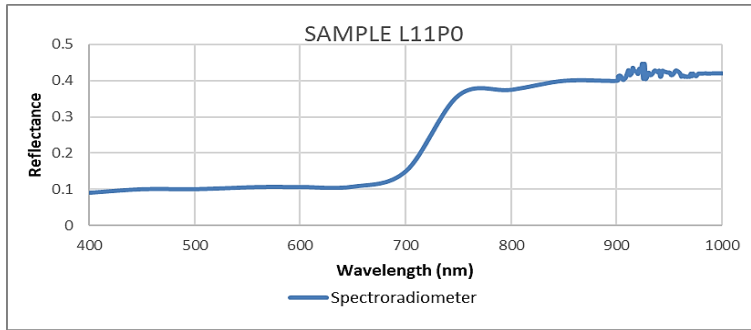
(r) Sample 18



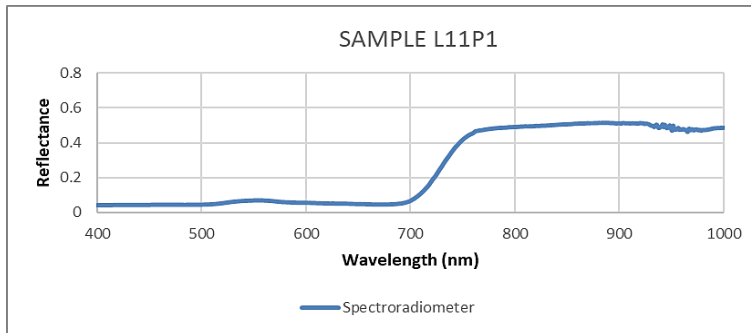
(s) Sample 19



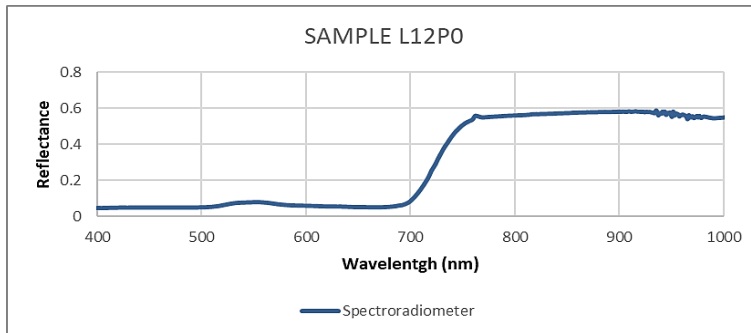
(t) Sample 20



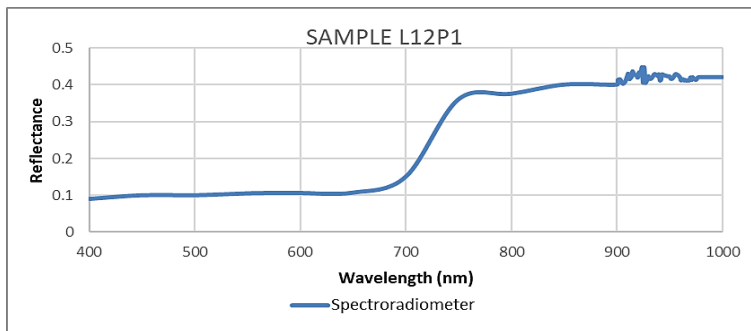
(u) Sample 21



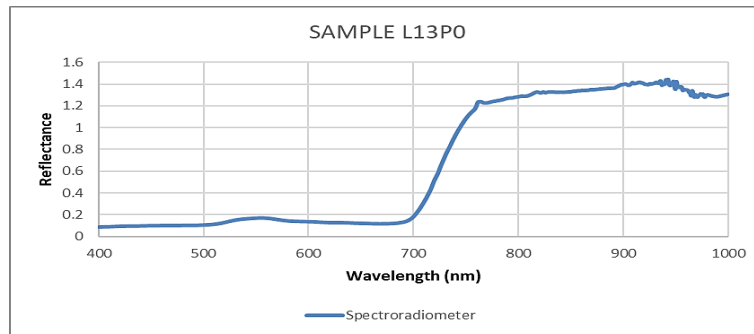
(v) Sample 22



(w) Sample 23



(x) Sample 24



(y) Sample 25

Figure 6. The spectral reflectance curve for 25 samples (6a – 6y) (L – Line, P – Point)

3.2 Vegetation Index

3.2.1 Normalized Difference Vegetation Index (NDVI)

Figure 7 presents an NDVI map as a series of colours corresponding to specific ranges of values. Red indicates bare soil or dead/sparse vegetation, and all shades of green indicate normal to dense vegetation cover. When the NDVI value is high, it shows it is healthier vegetation. Furthermore, NDVI values less than 0.1 denote barren rock, sand, or snow areas. Moderate levels (0.2 to 0.3) reflect shrub and grassland, whereas high values (0.6 to 0.8) represent temperate and tropical rainforests. Most of the examined region has a greener tint, indicating a high reflection of NIR light. As a result, nearly all the oil palm trees in the research region are in excellent and healthy condition.

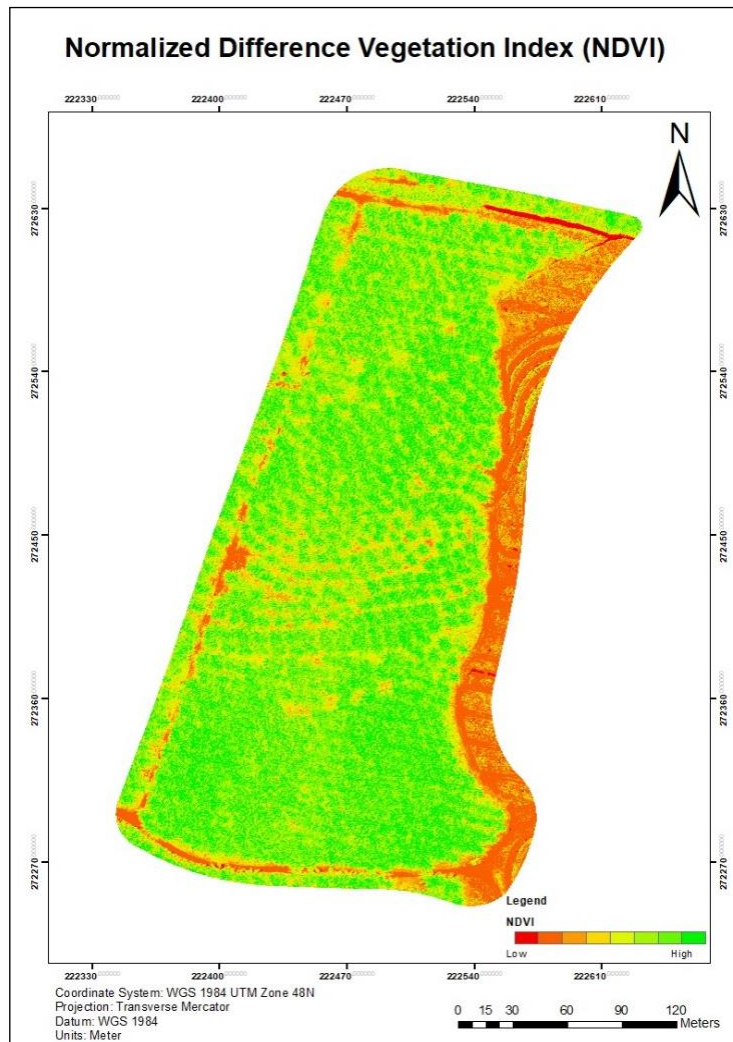


Figure 7. NDVI map of the study area

3.2.2 Modified Soil-adjusted Vegetation Index (MSAVI)

The Modified Soil Adjusted Vegetation Index (MSAVI) was developed to overcome limitations in applying NDVI to areas with a significant proportion of bare soil. MSAVI is utilized where indices such as NDVI produce inaccurate data, usually due to a lack of vegetation or chlorophyll. Moreover, MSAVI reduces the influence of bare soil on the SAVI (Soil Adjusted Vegetation Index). MSAVI is derived as a ratio of R and NIR values using an inductive L function to minimize soil impacts on the vegetation signal. Based on Figure 8, it is plain to observe that bare soil in the area of oil palm in Bukit Kledek represents a very high dispersion of greener colour. Furthermore, the near-zero value represents the bare soil area (non-vegetation). Meanwhile, the below zero (negative) value represents the low vegetation covered.

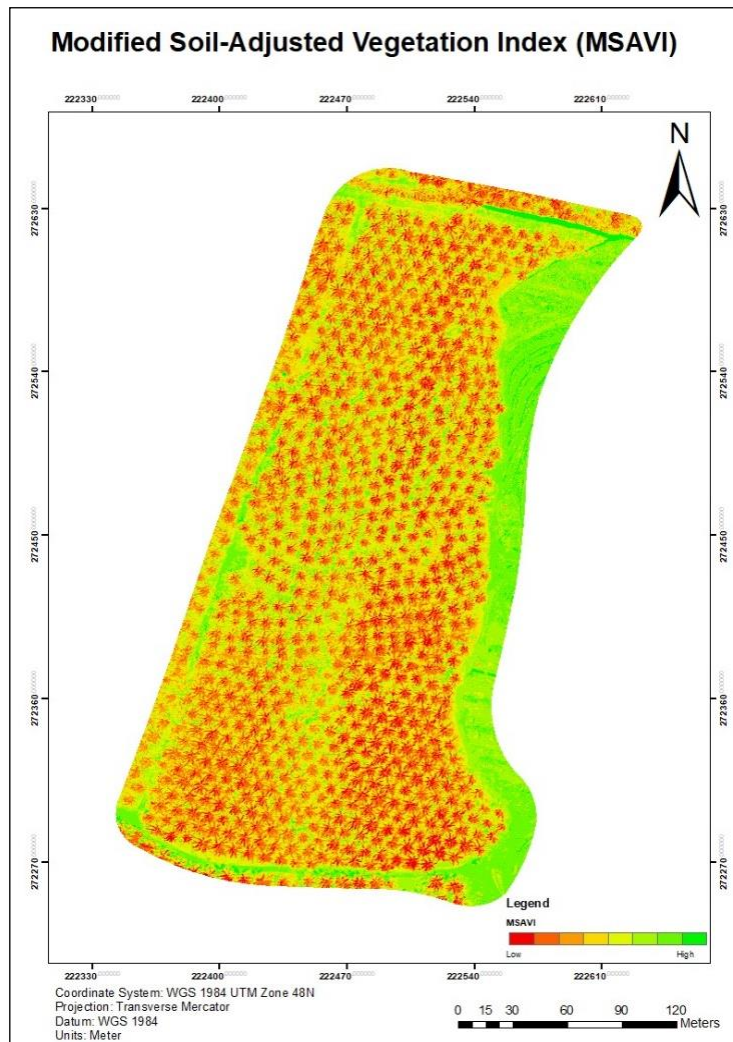


Figure 8. MSAVI map of the study area

3.3 Foliage Modelling

The result of the primary elements nutrients, which are Magnesium (Mg), Nitrogen (N), Phosphorus (P), Potassium (K), and Calcium (Ca), were calculated using orthophoto images based on regression analyses equation stated in Figure 9 until figure 13.

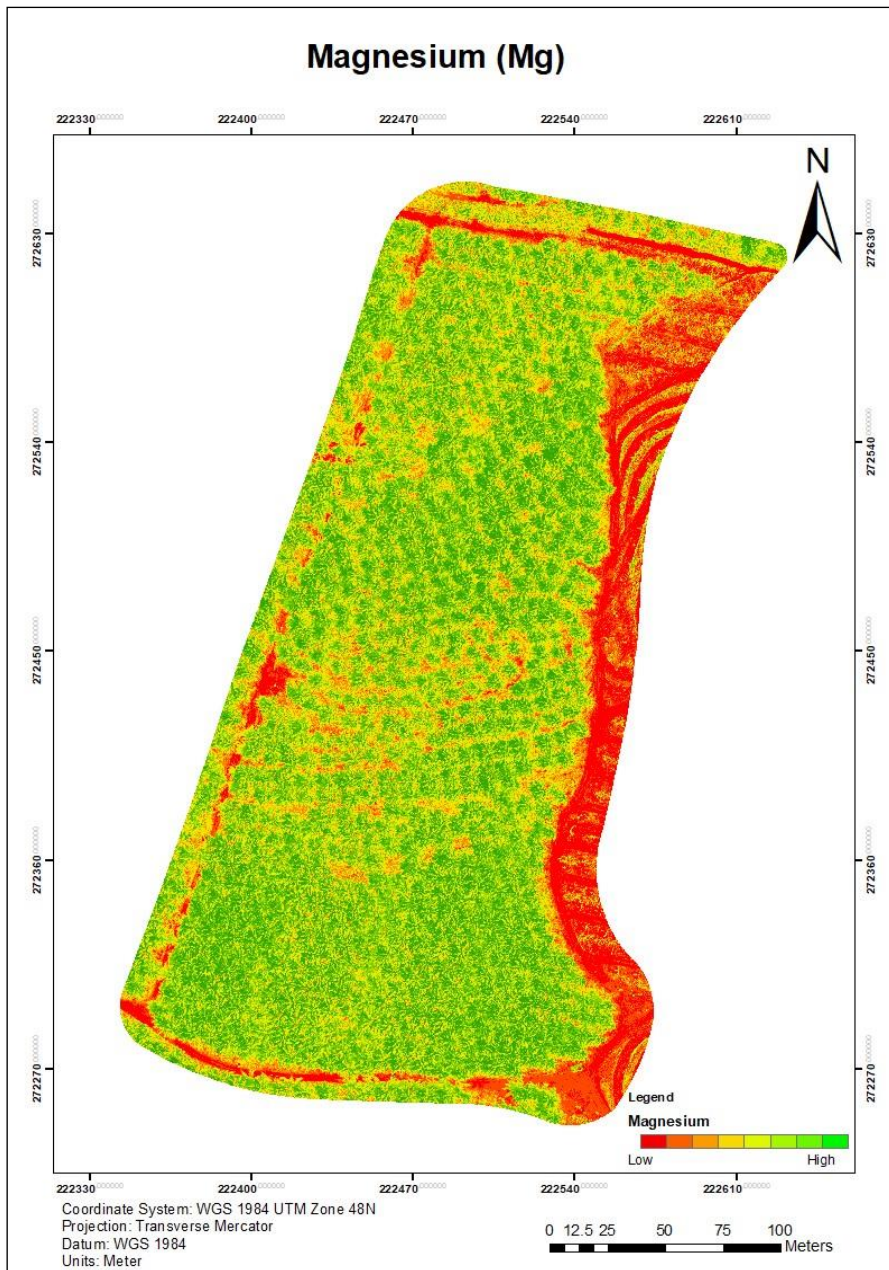


Figure 9. Magnesium map

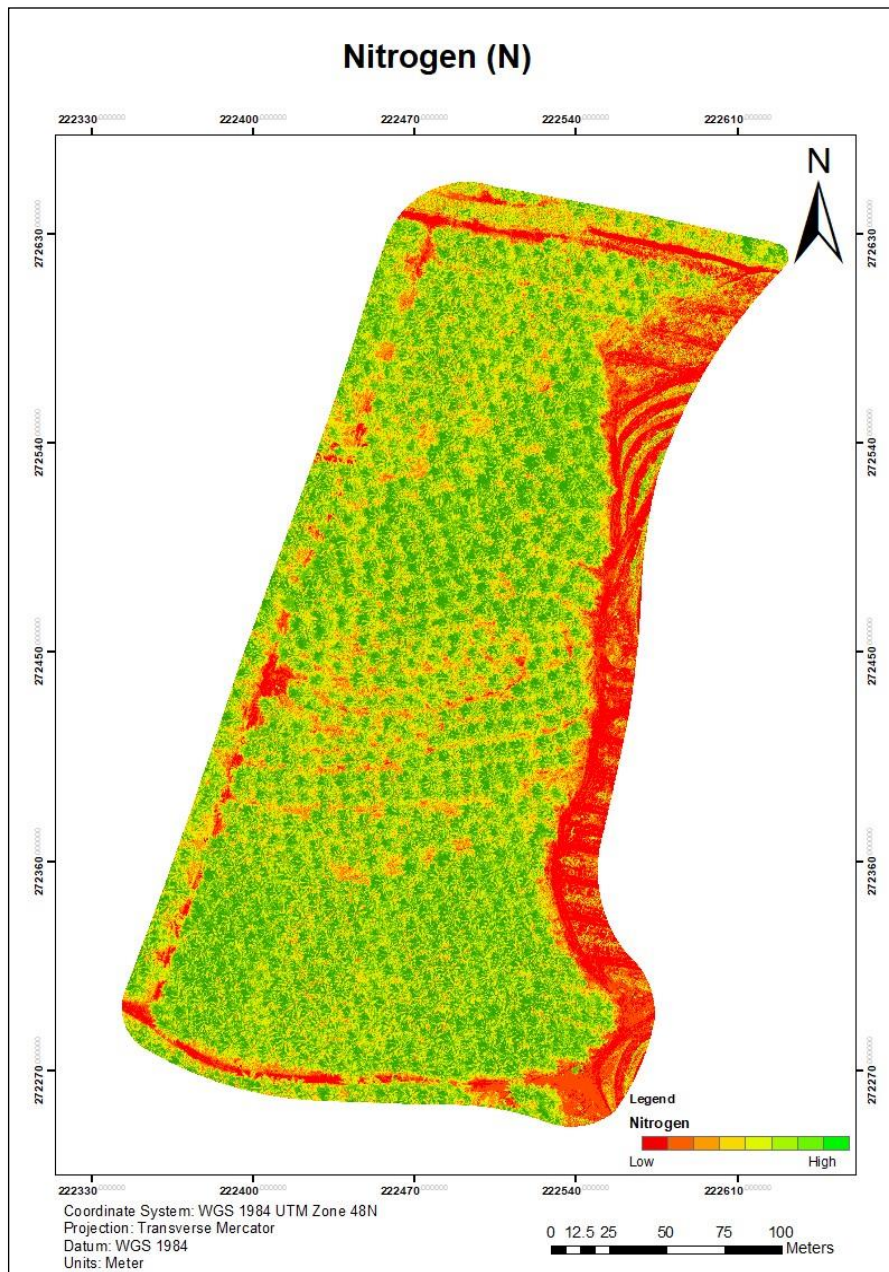


Figure 10. Nitrogen map

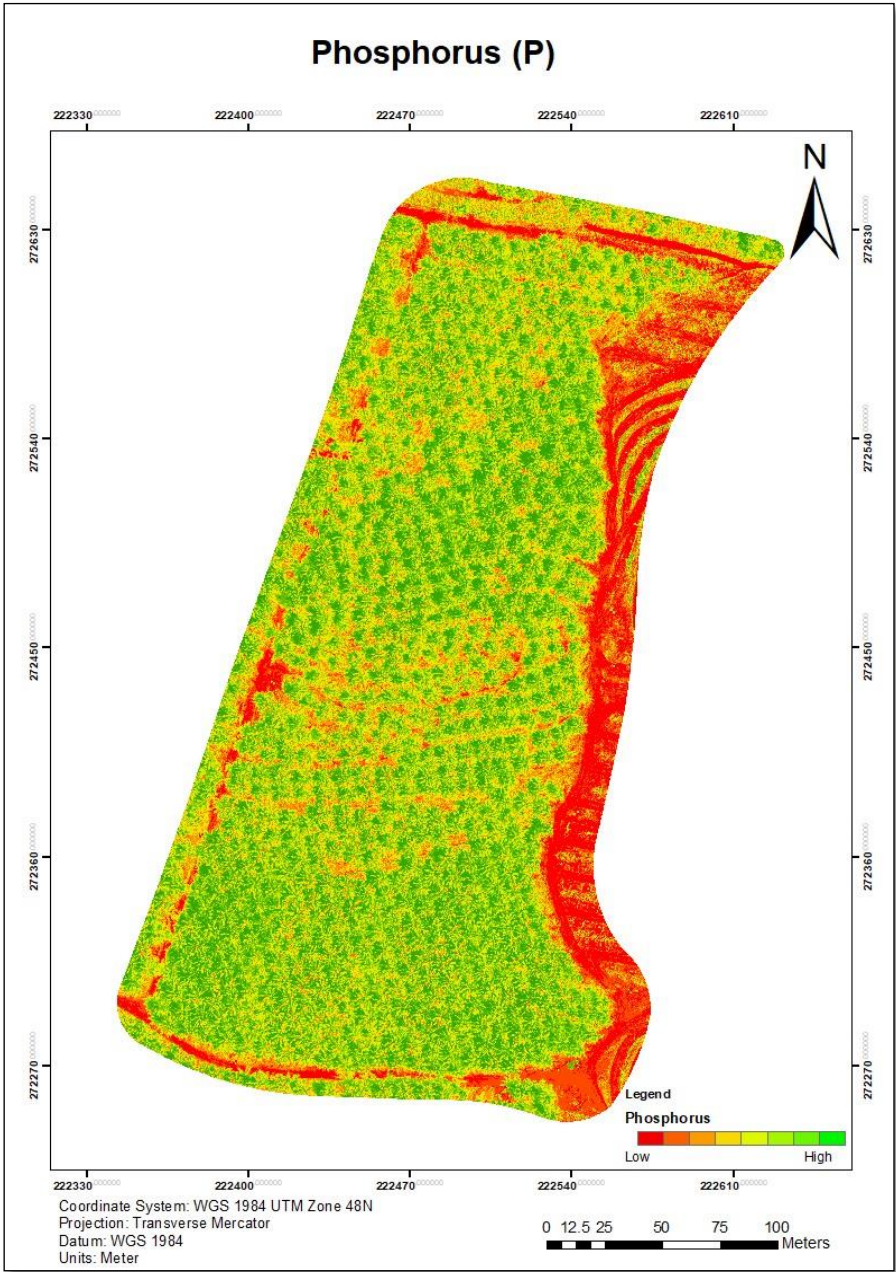


Figure 11. Phosphorus map

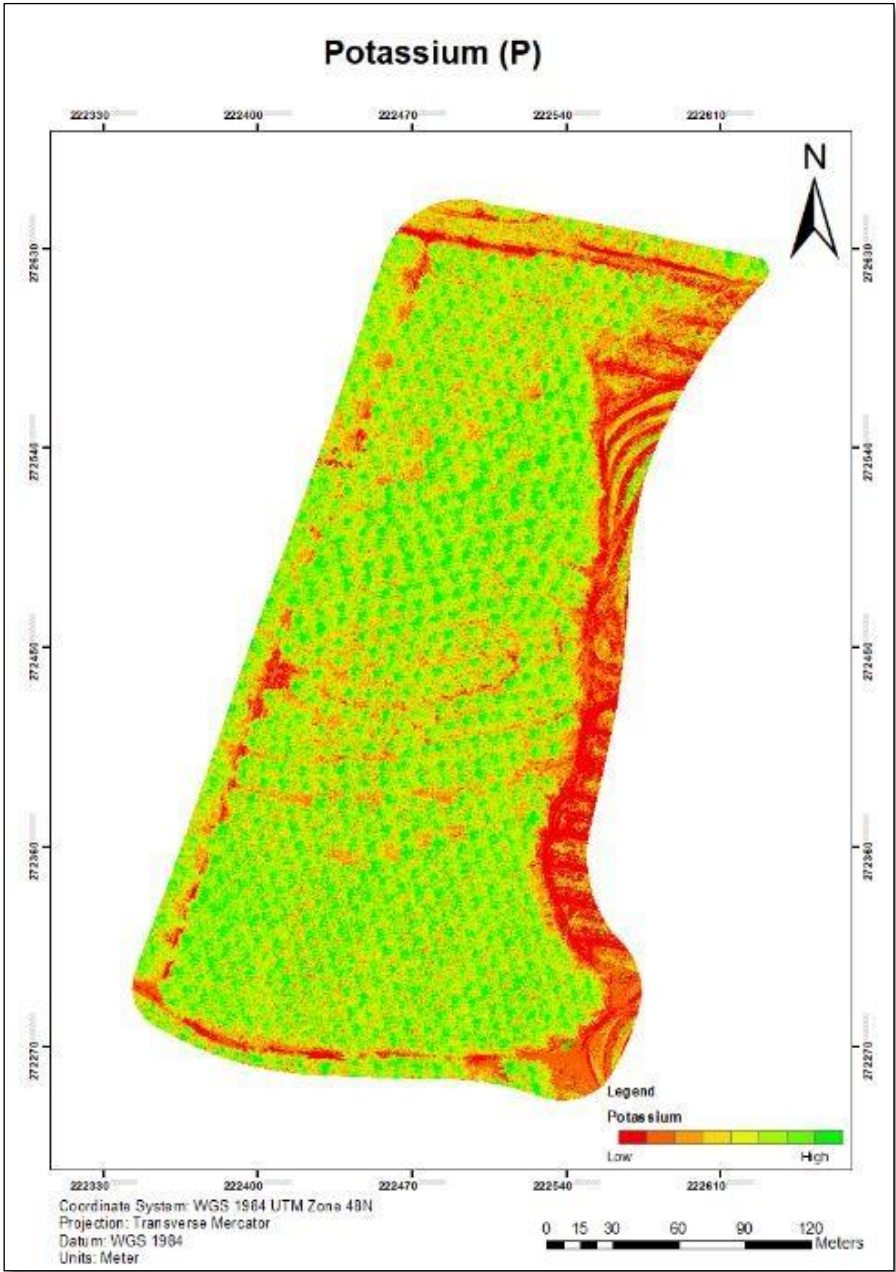


Figure 12. Potassium map

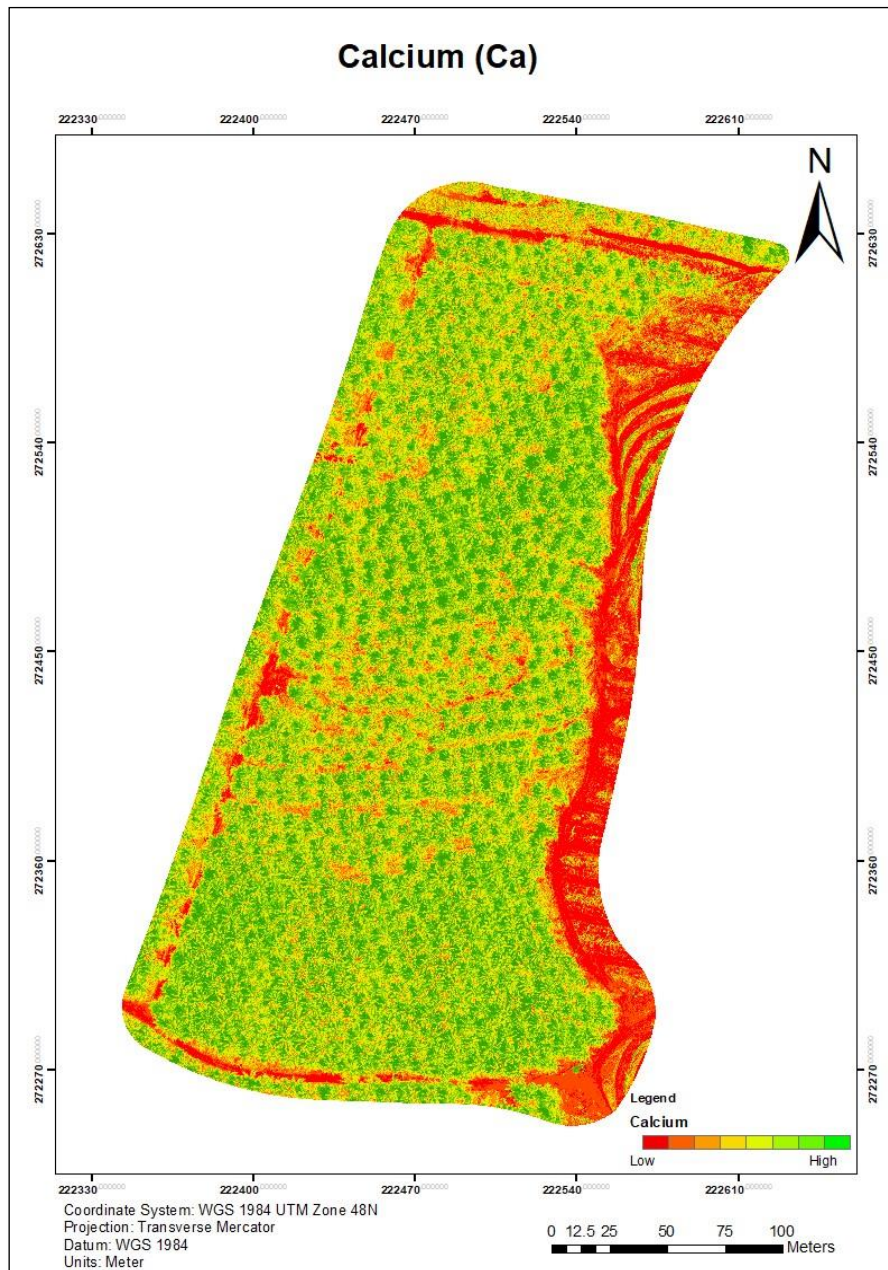


Figure 12. Calcium map

From the results, each element represents differences in values and slightly similar distribution patterns as seen in the maps. The differences may relate to external and internal factors, which cause bias, such as condition and sensor installation. Based on the result, we can notice that K concentration is relatively high in the research area since it shows a very high dispersion of greener colour than other nutrient elements. The photosynthetic activity of plants and their

chlorophyll molecules relies heavily on the mineral potassium. If there is enough potassium in the soil, it could protect crops from disease and drought. Due to the high concentration of leaf K in the research location, palms cannot absorb the low Mg concentration [8]. The age of the crop influences the concentration of N. Hence, the oil palms in the research region planted more than 12 years ago had an optimum concentration of leaf N, and the N deficit is unusual in mature palms [14]. The N deficiency in the research area is mainly caused by nitrogen loss through erosion, particularly on hilly terrain. Phosphorus is essential for crop growth and fruit quality. High levels of Al and Ca are the primary factors reducing P adsorption by palms in the studied area. Furthermore, soil pH and Mg content can alter Ca concentration in the leaf.

3.4 Quantitative Analysis

Random samples have been acquired for quantitative analysis, as shown in Figure 13 (without grid). The study will classify these samples into two groups: dependent and independent. T-test statistical analysis has been carried out, as shown in Table 3.

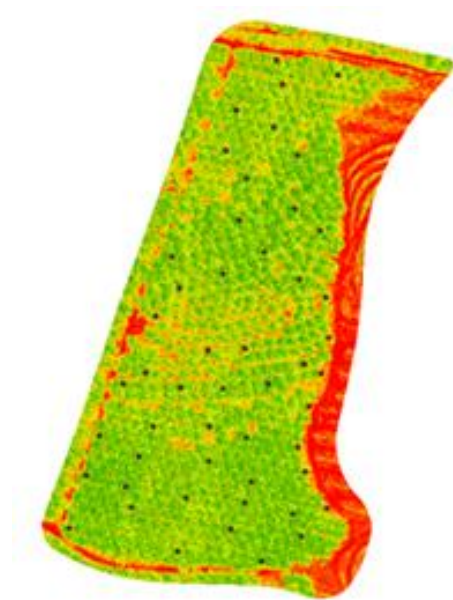


Figure 13. Distribution of dependent and independent sample points

Table 3. Dependent vs. independent samples

<i>T-Test of Nitrogen</i>		
t-Test: Paired Two Sample for Means		
	<i>Dependent</i>	<i>Independent</i>
Mean	41.87075226	31.74226799
Variance	92.57561538	43.68476039
Observations	25	25
Pearson Correlation	0.176667882	
Hypothesized Mean Difference	0	
df	24	
t Stat	4.747461813	
P(T <=t) one-tail	3.9461E-05	
t Critical one-tail	1.71088208	
P(T <=t) two-tail	7.89221E-05	
t Critical two-tail	2.063898562	

<i>T-Test of Phosphorus</i>		
t-Test: Paired Two Sample for Means		
	<i>Dependent</i>	<i>Independent</i>
Mean	1.544141557	1.171990211
Variance	0.120157853	0.059079489
Observations	25	25
Pearson Correlation	0.178994006	
Hypothesized Mean Difference	0	
df	24	
t Stat	4.819333435	
P(T <=t) one-tail	3.28732E-05	
t Critical one-tail	1.71088208	
P(T <=t) two-tail	6.57463E-05	
t Critical two-tail	2.063898562	

<i>T-Test of Potassium</i>		
t-Test: Paired Two Sample for Means		
	<i>Dependent</i>	<i>Independent</i>
Mean	-38.98980423	-32.06724792
Variance	35.58491546	21.62966934
Observations	25	25
Pearson Correlation	0.186162985	
Hypothesized Mean Difference	0	
df	24	
t Stat	-5.05497907	
P(T <=t) one-tail	1.80823E-05	
t Critical one-tail	1.71088208	
P(T <=t) two-tail	3.61647E-05	
t Critical two-tail	2.063898562	

<i>T-Test of Calcium</i>		
t-Test: Paired Two Sample for Means		
	<i>Variable 1</i>	<i>Variable 2</i>
Mean	11.04857071	7.997375603
Variance	7.670575771	4.003667927
Observations	25	25
Pearson Correlation	0.181839432	
Hypothesized Mean Difference	0	
df	24	
t Stat	4.90882325	
P(T <=t) one-tail	2.61912E-05	
t Critical one-tail	1.71088208	
P(T <=t) two-tail	5.23825E-05	
t Critical two-tail	2.063898562	

T-Test of Magnesium

t-Test: Paired Two Sample for Means

	<i>Dependent</i>	<i>Independent</i>
Mean	8.858978424	6.376286469
Variance	6.71068735	2.704299416
Observations	25	25
Pearson Correlation	0.164533589	
Hypothesized Mean Difference	0	
df	24	
t Stat	4.385216415	
P(T<=t) one-tail	9.91644E-05	
t Critical one-tail	1.71088208	
P(T<=t) two-tail	0.000198329	
t Critical two-tail	2.063898562	

Hypothesis:

H0: Dependent = Independent / $\rho = 0$

H1: Dependent \neq Independent / $\rho \neq 0$

From Table 3, a two-tailed paired samples T-test revealed that all the dependent samples are higher than independent samples in the vegetation with $t(24) = p \leq 0.05$. The p-value (0.000) is less than 0.05, it proves to reject the null hypothesis (H0) and H1 is accepted, where their sufficient evidence to conclude that the correlation is not equal to 0 and it is highly significant. It is shown that there is a significant linear relationship between dependent samples and independent samples as the population correlation coefficient of the nutrient is a positive correlation. As a result, dependent and independent samples of the five main elements nutrient involved in this study which is Nitrogen (N), Phosphorus (P), Potassium (K), Calcium (Ca), and Magnesium (Mg) can be simplified as in the Table 4.

Table 4. Statistical analysis results for nutrient elements

Parameter	RMSE
Nitrogen (N)	13.907
Phosphorus (P)	0.51
Potassium (K)	9.523
Calcium (Ca)	4.17
Magnesium (Mg)	3.499

The statistical analysis results in Table 4 show that the RMSE value, correlation of determination analysis, and R-square (r^2) give significant test results for all the nutrient elements, respectively. Based on the RMSE result, Phosphorus (P) has a better value than other parameters because an RMSE of 0.7 is small for a datum range of 0 to 1000 but not so small when the range is reduced to 0 to 1. Lower RMSE values, on the other hand, indicate better fit. The r^2 results show the positive linear to all elements. However, Magnesium (Mg) indicates a small positive linear association with a result of 0.499 compared to others, which indicates a large positive linear association. Furthermore, the t-test analysis at 95% confidence interval and degrees of freedom of 24 show that the parameters showed beyond the critical value of T at ± 2.060 (based on the student t distribution table) and rejected the null hypothesis due to very low p-values where it is shown that each nutrient parameter is not the same. The statistical analysis above indicates that each parameter has a strong correlation and is powerfully relevant to the produced trend model of nutrient elements in this study using a drone-based remote sensing technique.

3.5 Qualitative Analysis

Three parameters have been analyzed qualitatively, as shown in Figure 14.

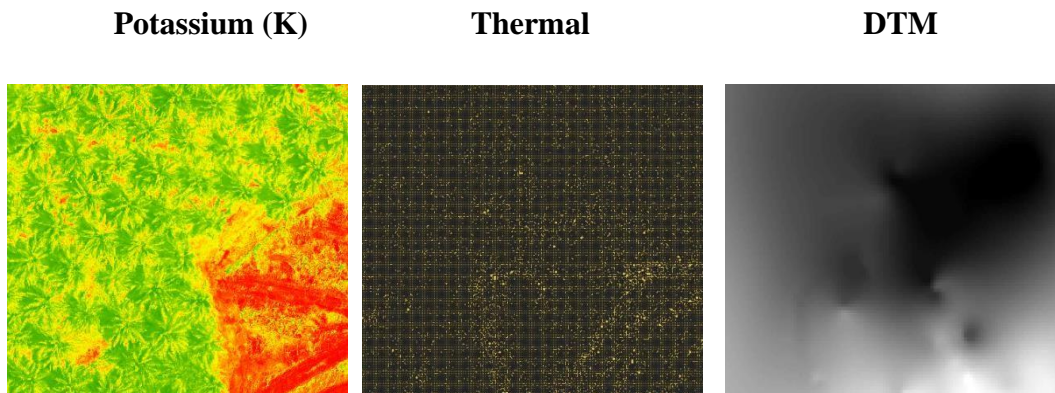


Figure 14. Potassium, thermal and DTM image for one sample

According to a previous study that focused on the relationship between elevation and temperature, temperature tended to decrease with increasing elevation. Each plant type has different minimum, optimum and maximum temperature limits for each level of growth [11]. Temperatures below minimum or above the maximum will inhibit plant growth and development.

However, there is a consistent decreasing trend in near-surface temperature with increasing elevation, which acts on the surface heating processes via the heat exchange process between the surface and the air [13].

From the foliage analysis result, the potassium is high in the study area since it shows a very high dispersion of greener colour than other nutrient elements. This is because potassium plays an important role in converting light into biochemical energy during photosynthesis. Potassium application increased the leaf area of oil palms. Leaf area is related to how much sunlight the leaves in photosynthesis can capture. The optimum leaf area would increase the assimilate formed so that it would affect the yield of oil palm.

Since photosynthesis is a chemical reaction, and the rate of most chemical reactions increases with temperature, it is also relevant to the rate of photosynthesis, where higher temperatures typically result in a greater rate of photosynthesis. In tropical climates, literature on subsurface soil temperature indicates temperatures can range from 15 to 25 °C below ground [16]. Tropical climates are characterized by year-round monthly average temperatures of at least 18 °C (64.4 °F) and sweltering. Typically, the annual temperature range in tropical climates is relatively modest. In addition, there is a strong correlation between elevation and temperature, with a lapse rate of approximately 6 °C per 1000 m, and elevation is frequently associated with slope inclination in tropical regions [17].

4.0 Conclusion

The study shows that nutrient content can be detected using the remote sensing technique. The ability of remotely sensed data to quantitatively detect and estimate the nutrient concentration in the soil would enhance yield predictions and provide farm managers with valuable information for making day-to-day management decisions. A spectroradiometer could be used to validate the spectral reflectance from multispectral images if the reflectance of the images exhibits the same trend as the spectroradiometer's reflectance. Hence, this study promotes a transformation from the traditional, time-consuming and expensive method of soil analysis to this new technique of data analysis. Compared to foliar research conducted in oil palm plantations using block samples, the nutrient mapping developed in this study is substantially superior in capturing and displaying the spatial variability of nutrient concentration. Moreover, using regression analysis, the relationship between the dependent and independent variables is examined to determine the optimal range of

EMR, which is the most sensitive to nutrients, and the results indicate that each parameter has a strong correlation. In conclusion, deploying UAVs with multispectral cameras will enable the building of trend models for nutrient elements using remote sensing techniques.

Acknowledgement

The authors would like to express high appreciation to Tradewinds Plantation Berhad and Faculty of Built Environment and Survey, Universiti Teknologi Malaysia (UTM). Big thank you to Mr Abdul Manap bin Mahpob from Geolatitude Sdn Bhd, Johor for helping with technical issue and Mr Mohd Jefri bin Mamat for helping at the plantation during data collection. The authors would like to thank all the individuals involved in the study who gave their best support. Finally, the authors would like to express their gratitude for the financial support provided under grant funding through VOT RJ130000.7652.4C585 and UTMICON 3.0 UTM Caps Drone: UTM Campus Autonomous Patrol And Surveillance System under Project 1 VOT Q.J130000.4352.09G75.

REFERENCE

- [1] Agassi, E., & Ben-Yosef, N. (1997). Relation between thermal infrared and visible/near infrared images of ground terrain. *Optical Engineering*, 36(3), 862-873. <https://doi.org/10.1117/1.601141>
- [2] Ariff, M. F. B. M. (2017). Project Planning. *Faculty of Built Environment and Surveying*. Universiti Teknologi Malaysia.
- [3] Astina, T. (2015). Oil Palm Monitoring By Using UAV. *Degree of Bachelor of Engineering (Geomatics)*. Universiti Teknologi Malaysia (UTM)
- [4] Azid, N. S. B. (2014). Photogrammetry Lecture 5: Flight Planning. *Faculty of Civil Engineering*. Universiti Teknologi Malaysia
- [5] Behera, S. K., B. N. Rao, K. Suresh, K. Ramachandrudu & K. Manorama (2016) Soil fertility, leaf nutrient concentration and yield limiting nutrients in oil palm (*Elaeis guineensis*) plantations of Surat district of Gujarat. *Indian Journal of Agricultural Sciences*, 86, 409-413.
- [6] Bryan D. See, Shaiful J. Hashim, Helmi Z. M. Shafri, Syaril Azrad & M. R. Hassan (2018) A new rapid, low-cost and GPS-centric unmanned aerial vehicle incorporating in-situ multispectral oil palm trees health detection. *J Agric Sci Bot 2018*, Volume 2, 12.

- [7] Chong, K. L., Kanniah, K. D., Pohl, C., & Tan, K. P. (2017). A review of remote sensing applications for oil palm studies. *Geo-spatial Information Science*, 20(2), 184-200. <https://doi.org/10.1080/10095020.2017.1337317>
- [8] Ibrahim, A. L., Hashim, M., Rasib, A. W., Ali, M. I., Kadir, W. H. W., Sumairi, M. R., & Haron, K. (2003). Detection of foliar nutrients of oil palm crop using remote sensing. In *Proceedings of the KSRS Conference* (pp. 558-560). The Korean Society of Remote Sensing.
- [9] Jayaselan, H., Nawi, N., Ismail, W., Shariff, A., Rajah, V., & Arulandoo, X. (2017). Application of spectroscopy for nutrient prediction of oil palm. *Journal of Experimental Agriculture International*, 15(3), 1-9. <https://doi.org/10.9734/JEAI/2017/31502>
- [10] Kushairi, A., Loh, S. K., Azman, I., Hishamuddin, E., Ong-Abdullah, M., Izuddin, Z. B. M. N., ... & Parveez, G. K. A. (2018). Oil palm economic performance in Malaysia and R&D progress in 2017. *J. Oil Palm Res*, 30(2), 163-195.
- [11] Woittiez, L. S., Haryono, S., Turhina, S., Dani, H., Dukan, T. P., & Smit, H. (2016). Smallholder Oil Palm Handbook Module 4: Fertiliser Application.
- [12] Norasma, C. Y. N., Fadzilah, M. A., Roslin, N. A., Zanariah, Z. W. N., Tarmidi, Z., & Candra, F. S. (2019, April). Unmanned aerial vehicle applications in agriculture. In *IOP Conference Series: Materials Science and Engineering* (Vol. 506, p. 012063). IOP Publishing. <https://doi.org/10.1088/1757-899X/506/1/012063>
- [13] ra Özbay, B., Esin, Y. E., & Çengel, F. (2015, June). Specific band ratio for vegetation indices calculation in hyperspectral images. In *2015 7th Workshop on Hyperspectral Image and Signal Processing: Evolution in Remote Sensing (WHISPERS)* (pp. 1-4). IEEE. <https://doi.org/10.1109/WHISPERS.2015.8075383>
- [14] Tarmizi, A. M., & Mohd Tayeb, D. (2006). Nutrient demands of tenera oil palm planted on inland soil of Malaysia. *Journal of Oil Palm Research*, 18, 204.
- [15] Wahid, M. B., Abdullah, S. N. A., & IE, H. (2005). Oil Palm—Achievements and Potential. *Plant Production Science*, 8(3), 288-297. <https://doi.org/10.1626/pps.8.288>
- [16] Wear, J. I., & Cope, J. T. (1976). Relationship between soil test values and analysis of pecan leaves taken at three dates. *Communications in Soil Science and Plant Analysis*, 7(3), 241-252. <https://doi.org/10.1080/00103627609366637>

- [17] Albakri, Z. M., Kassim, M. S. M., Abdullah, A. F., & Harith, H. H. (2019). Analysis of Oil Palm Leaf Phyllotaxis towards Development of Models to Determine the Fresh Fruit Bunch (FFB) Maturity Stages, Yield and Site-Specific Harvesting. *Pertanika Journal of Science & Technology*, 27(2).